ISFV13 - 13th International Symposium on Flow Visualization
FLUVISU12 - 12th French Congress on Visualization in Fluid Mechanics
July 1-4, 2008, Nice, France

THERMAL PLUMES VISUALISATION: DIFFERENTIAL INTERFEROMETRY VERSUS THERMOCHROMIC LIQUID CRYSTALS

Angela Limare*, Ichiro Kumagai, Judith Vatteville*, Anne Davaille*'*****
***Institut de Physique du Globe de Paris, France**
**** Earthquake Research Institute, University of Tokyo, Japan**
***** Laboratoire FAST, CNRS / Univ. P6 / Univ. Psud, Orsay, France**

KEYWORDS:
Main subject(s): *Earth's mantle convection, Thermal plumes*
Fluid: *sugar syrup, silicone oil*
Visualization method(s): *Differential interferometry, Thermochromic Liquid Crystals*
Other keywords: *viscous fluids dynamics*

ABSTRACT: *Our planet Earth is cooling through thermal convection in its solid 3000 km thick upper part (the "mantle"). Given the mantle characteristics, laminar thermal plumes should develop out of the hot thermal boundary layer located at the bottom of the mantle. For several decades, much effort has been done to understand plume dynamics and to provide scalings for plume ascent velocity or for plume growth by entrainment of ambient fluid. However, different studies have often proposed different scaling laws. The source of scalings discrepancy, besides the differences in experimental setups, originates from the fact that the plume definition often depends on the visualization technique used.*
Here we study the dynamics of a plume generated from a small heat source, using two visualisation techniques allowing the quantitative determination of the temperature field: Differential Interferometry (DI) and Thermochromic Liquid Crystals (TLC). This comparative study allowed us to determine the advantages and disadvantages of each technique, to quantify the differences among possible definitions of a thermal plume, and to identify the different stages in plume development.

1 General Introduction

Intra-plate volcanism on Earth, such as Hawaii or La Reunion volcanic islands, is interpreted as a consequence of rising hot plumes generated deep in the solid 3000 km-thick Earth's silicate mantle. These plumes constitute a unique opportunity to probe the deep interior of our planet. But in order to decipher the information they bring to the surface, we need to understand their dynamics. Up to now, studies of plumes in viscous fluids have focused a) experimentally on global features such as volume and ascent rate of the plume head, and b) theoretically on stem temperature and velocity structure (see [1] for a review). However, the different setups and the different techniques used to determine the plume shape (distribution of dye [2], small tracer bubbles [3], shadowgraph [4], differential interferometry [5] and isotherms by Thermochromic Liquid Crystals [6]) led to different scaling laws and to diverging explanations about entrainment in head and tail. Hence, it is essential to investigate

how the technical differences and underlying assumptions influence our understanding of plume dynamics. Here we study plume dynamics using two different visualisation techniques allowing the quantitative determination of the temperature field: Differential Interferometry (DI) and Thermochromic Liquid Crystals (TLC).

On geological time scales (10^8 yrs), mantle material flows, convects, and as a first approximation can be considered as Newtonian, whereby stress increases linearly with strain rate. Moreover, solid-state creep is thermally activated, whereby mantle material viscosity decreases strongly with increasing temperature (a 100°C increase typically results in a 10-fold viscosity decrease). Hot mantle plumes are often associated with a 300°C temperature increase compared to the ambient mantle, and therefore should be 1000 times less viscous. The dynamical regime of interest is therefore one of a) high Prandtl number (Pr~10^{23} in the mantle), b) high Rayleigh number (> 10^6) so that convective plumes can develop, and c) strongly temperature-dependent viscosity.

In this study, we focus on the development of a laminar thermal plume generated from a local heat source. Two fluids were used: silicone oils whose viscosity depends weakly on temperature, and sugar syrups, whose viscosity depends strongly on temperature. The Prandtl number was always greater than 5000 (i.e. no inertial effects in our tank, as in the mantle), and the viscosity ratio between the colder and hotter parts of the fluid ranged between 1.5 and 60.

2 Experiment

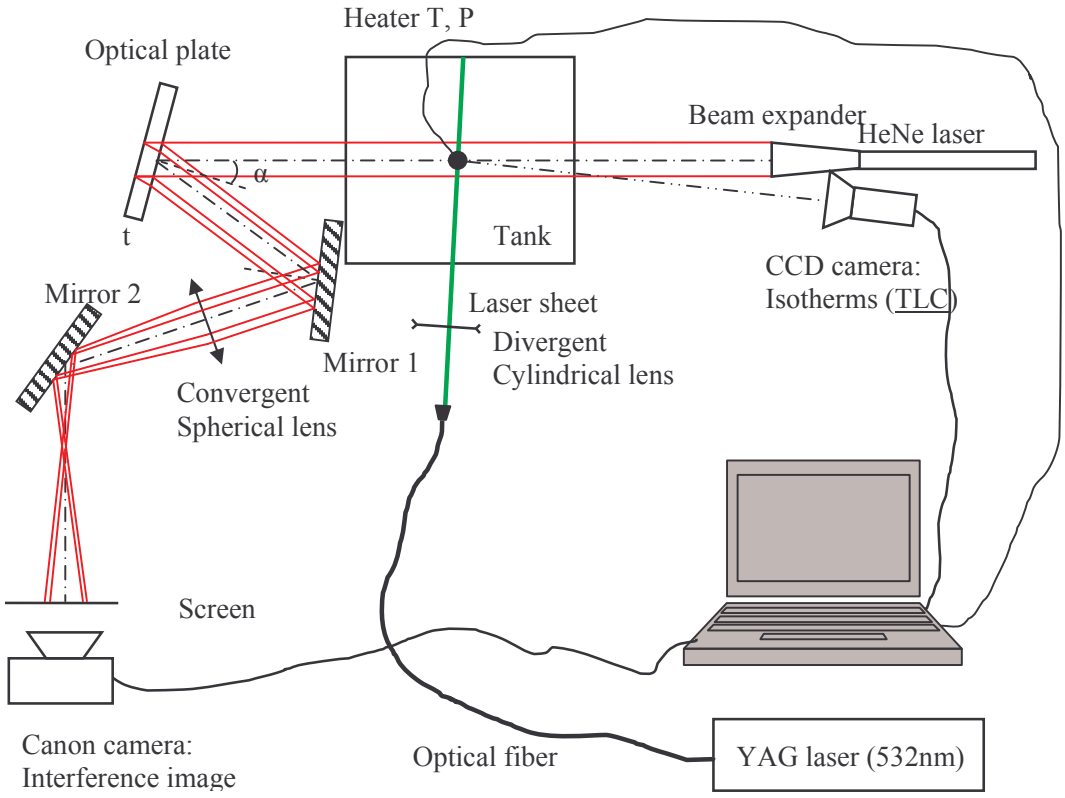

Fig.1. Experimental setup

2.1 Experimental setup

Figure 1 shows the experimental setup for simultaneous temperature measurements by DI and TLCs. Two sets of experiments were carried out. The first set uses glucose syrup (GS6075 from Syral) and a Peltier element covered by a 4mm thick, 25mm diameter Cu disk as a heating source. The second set uses silicone oil (47V5000 from Caldic) and a Peltier element covered by a 4mm thick, 18mm diameter Cu disk as a heating source. The physical properties of the fluids were measured in the laboratory, except for the heat capacity (Table 1 and Fig.2). For each experiment, the Peltier heater is switched on at time t=0 and a constant voltage applied to it throughout the experiment. The temporal evolution of the thermal plume is then monitored simultaneously through differential interferometry and liquid crystal visualization. Both the ambient temperature and the temperature of the Peltier heater surface, measured by thermocouples, and the electric current voltage and intensity, are monitored through time.

Property	sugar	oil
η (20°C)	11.95	5.00 (Pa.s)
κ	0.9×10^{-7}	1.3×10^{-7} (m^2/s)
C_p	3159	1460 (J/kg/K)
ρ (20°C)	1386	973 (kg/m^3)
α	5.81×10^{-4}	9×10^{-4} ($°K^{-1}$)
dn / dT	-2.05×10^{-4}	-3.71×10^{-4} ($°K^{-1}$)

Table 1: Physical properties of the fluids: η ,viscosity; κ, heat diffusivity; C_p, heat capacity; ρ, density; α, thermal expansion; n, refraction index.

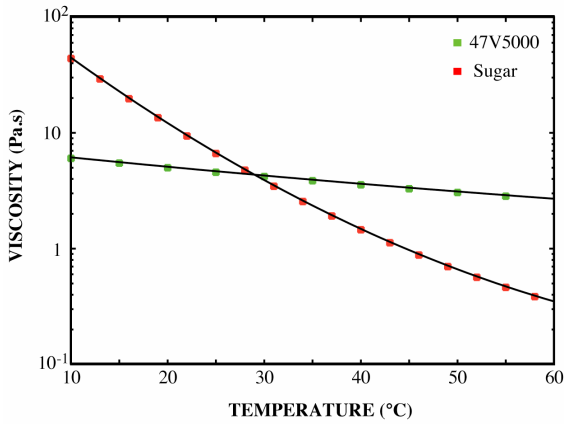

Fig.2: Viscosity of the silicone oil and of the sugar syrup as a function of temperature.

2.2 Differential interferometry

Differential interferometry (also called shearing interferometry) is a method to measure derivatives of light phase distortions. This is done by the interference between a beam passing through the object and the same beam laterally displaced. The simplest way of producing these two beams is to use an optical flat plate tilted at a certain angle [5]. A HeNe expanded laser beam was used as a light source for the DI experiment. Behind the tank was placed the tilting plate (thickness t=4.16mm and refractive index n_p=1.51872), inclined at an incidence angle α of 10.5°C (Fig.1). Without any object, the displacement δ introduced by the tilting plate [7]:

$$\delta = 2t / \sqrt{\sin\alpha \cdot \cos\alpha \cdot n_p^2 - \sin^2\alpha} \qquad (1)$$

produces a uniform interferogram, the orientation of fringes being perpendicular to the tilt plane and their frequency related to δ. Therefore the sensitivity of the method can be varied. The interferograms

were registered through time with a digital camera (Canon 8.2Mpixels). Vertical fringes follow horizontal temperature gradients. The fringes away from the plume correspond to light propagation through uniform background (fig.3A).
The differential interferometry has several advantages:

1) Its variable sensitivity: carrier fringe orientation and frequency can be chosen separately. So that it is possible to visualize with the same apparatus the flow configuration in two fluids with very different temperature-dependence of the refractive index. Moreover, the separation between the object and the interferometer facilitates the investigation of large and complicated objects. The dimensions of investigated objects are only limited by the diameter of the exit lens of the beam expander (80mm in our case).

2) The method does not require high quality optics as Mach Zender interferometry for instance. In the absence of the object, we obtain a uniform interferogram of vertical fringes indicating constant horizontal gradients. In reality the initial interferogram is not completely uniform since the tank does not have walls of optical quality and the beam expander quality is relatively poor. This, however, will not affect the result since for the interferogram analysis in the presence of the thermal anomaly only the differences between the fringes positions matter.

3) For axisymmetric objects, the spatial distribution of the refractive index can be obtained easily because the Abel inversion formula is reduced to a simple integration, which can be done more reliably than a differentiation. In that respect, differential interferometry results are less noisy than Mach-Zender interferometry, where the spatial distribution of the refractive index is obtained through numerical differentiation of the optical path difference. But the Abel transform can be applied only under the assumption that the probing rays are straight lines, which is almost never the case in practice. If the second or higher derivatives of the optical anomaly are of appreciable value, a shadowgraph picture will be superposed on the recording plane [5]. However, for strongly refracting axisymmetric objects it has been shown [8] that Abel inversion yields rather accurate results if the interferogram is formed with appropriate imaging. The convergent lens introduced into the pathway forms the image of the centre plane of the object on the screen. The positioning of the lens ensures a 1:1 object to image ratio. But since the test region is imaged its position has to be well determined in advance.

The differential interferometry is a projection method; the image obtained onto the screen contains integrated information of the phase object. The Abel transform is used to project an optically thin, axially symmetric emission function onto a plane and the reverse Abel transform is used to calculate the emission function given a projection. In our case the emission function is proportional to the refractive index distribution introduced by the object:

$$\frac{2\pi}{\lambda}(n(r)-n_0) = -\frac{1}{\pi\delta}\int_r^\infty \frac{d(y)dy}{\sqrt{y^2-r^2}} \qquad (2)$$

where d(y) is the result of the interferogram evaluation calculated as follows: The evaluation of the interferogram can be done by Fourier analysis, and the result, being the first derivative of the integral phase shift caused by the object is obtained with high accuracy. From the intensity profile of the interferogram along one straight horizontal line (Fig.3A), the phase function is calculated. The difference in phase between each consecutive fringe is 2π radians (180°). For the initial interferogram the phase function is a straight line as a function of the pixel number (h0 in Fig3.B). When the object is present, the phase function will be distorted (h in Fig3.B), and the difference between the two lines is d(y). The refractive index distribution introduced by the object can be calculated numerically by simple

integration (Eq. 2; Fig.3D). Then, knowing the temperature dependence of the refractive index, the temperature field can be calculated (Fig.3E). In order to compare the DI and TLC temperature results, the DI temperature field was intersected to the discrete values of the isotherms and their positions into the plume were identified. To apply the analysis described here, the flow has to be laminar.

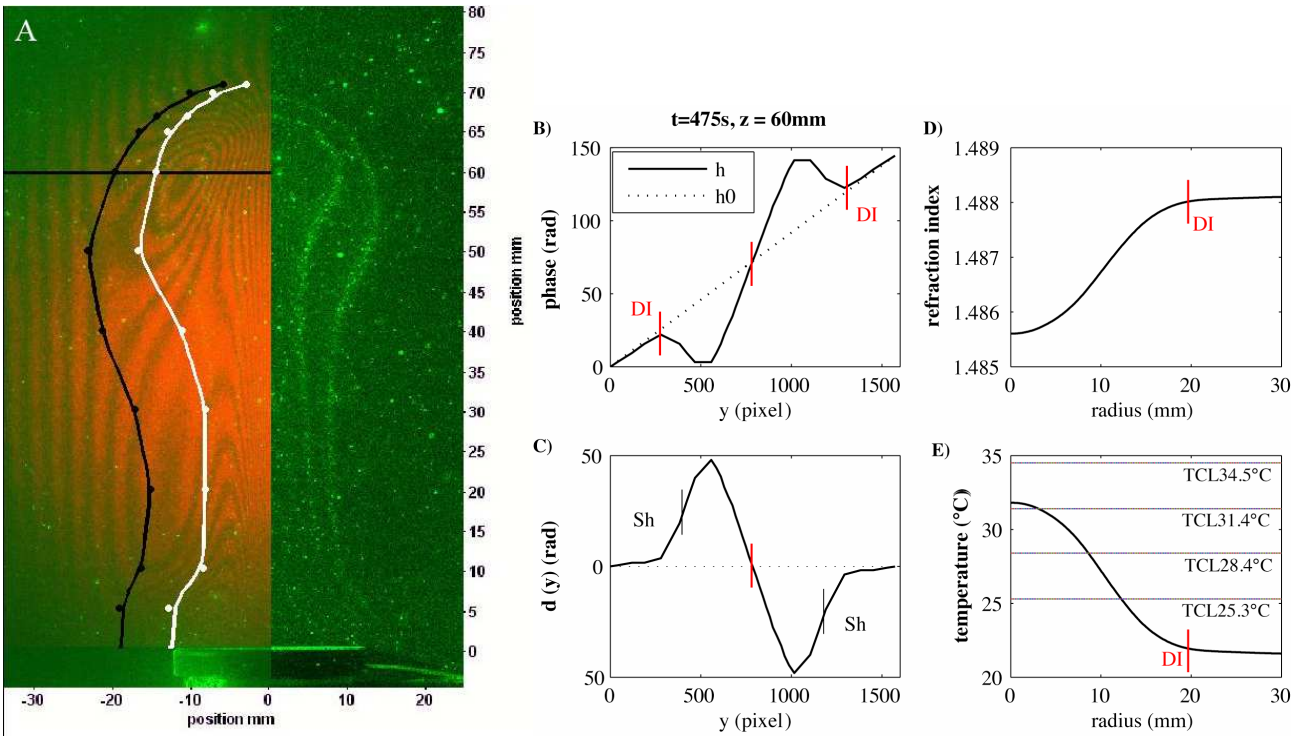

Fig.3. Sugar syrup plume at t=475 sec and power P=1.46W. A) Right: the bright lines are the isotherms. Left: differential interferometry image. The black line shows the contour of the non-zero thermal anomaly ("DI" on Fig.3B, D, E). The white line shows the contour of a "shadowgraph" defined as location of maximum phase displacement derivative ("Sh" on Fig.3C). B) Phase on a horizontal cross-section at 60mm height. C) Phase difference (d) between the distorted interferogram (h) and the initial one (h0). D) refractive index distribution, and E) temperature field as a function of radius.

2.3 Thermochromic Liquid Crystals (TLC)

The use of TLC allows temperature mapping on a 2D-plane in the fluid flow without perturbing it [9-11]. When illuminated by white light, TLC colour changes with increasing temperature from colourless to red at low temperatures, passes through green and blue to violet and turns colourless again at high temperatures. The total temperature range ΔT_c accessible with one TLC is between 1 and 40°C. With a high precision colour CCD camera, a very stable white light and a precise calibration of the TLC colour against true temperature, it is then possible to determine the temperature field with a 5% precision over ΔT_c [12]. Since a) thermal convection in viscous fluids involves typical temperature heterogeneity of 20 to 60°C, and b) we want a temperature precision better than 1°C (5%), we choose

to seed the experimental cell with several types of TLCs, each reflecting light at a different temperature, and to illuminate a cross-section of the tank with a monochromatic laser light sheet. Therefore each type of TLC is responsible for one bright line, which represents an "isotherm" (Fig.3A, 5, 6). This method was previously used to study two-layer convection [13], plumes out of a viscous thermal boundary layer [14] and plumes out of localised heat source [6]. It can be combined with Laser Induced Fluorescence and Particle Image Velocimetry to get simultaneously the composition and velocity field [6].

Here, the sugar syrup was seeded with five types of liquid crystals (20-30µm aqueous slurries) and the silicone oil with two types of TLC (20-30µm powder). A cross-section of the experimental tank is illuminated by a 532nm YAG (Coherent VERDI 2W) laser sheet 1 mm-thick. The scattered light from the liquid crystals was then recorded by a black and white CCD camera (LaVision 1280x1020 pixels).

The TLCs were calibrated by imposing a stable linear temperature gradient to a 10 cm layer of the experimental fluid: the light intensity across a vertical cross-section of the tank is then plotted as a function of the vertical profile of temperature (Fig.4). Each type of TLC results in an intensity peak for a given temperature. Each bright stripe has a finite thickness because the polymeric capsules enclosing the TLCs introduce some scatter around the temperature at which they respond. The peak maximum gives us the "isotherm" value (Table 2); and the width of the peak at half maximum intensity (or "bandwidth") gives the "local temperature gradient" (Table 2). Peaks are much better defined for aqueous slurries in sugar syrups, where the precision of the isotherms' values can reach ±0.1°C, and the bandwidth is about 0.2°C. Results in silicone oils are poor in comparison (Table 2 and Fig.4), with smaller light contrast and much broader peaks. This could be due to the different nature of the coating layer of TLC capsules: gelatine for TLC for oils and urea resin for aqueous slurries.

Product name	Peak value	Bandwidth
In sugar:		
KMN37-39	37.5 °C	0.20 °C
KMN34-36	34.5 °C	0.20 °C
KMN31-33	31.4 °C	0.14 °C
KMN28-30	28.4 °C	0.17 °C
KMN25-27	25.3 °C	0.23 °C
In oil:		
RM24-26	24.1 °C	1.0 °C
RM33-35	34.8 °C	1.5 °C

Table 2: Types of liquid crystals (from Japan Capsular Products, Inc.) used in the experiments with their calibration values.

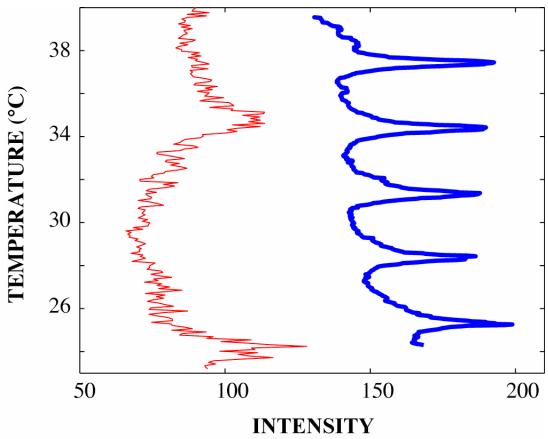

Fig.4: TLC calibration. Light intensity as a function of temperature. Red=silicone oil; blue=sugar syrup.

3 Results and discussion

3.1 Temperature field determination: DI versus TLCs:

The images from the two cameras were simultaneously recorded. Movies 1 and 2 show the development of a thermal plume as seen by DI (on the left of the screen) and by TLC (on the right), in sugar syrup (Mov.1, Fig.3 and Fig.5) and in silicone oil (Mov.2, Fig.6).

DI: The differential interferograms are inverted, using the procedure described in section 2.2 and Fig.3, to determine the complete temperature field. On Fig.3, the center of the plume is determined as the point where the two phase functions are intersecting and corresponds to phase difference d(y)=0 (Fig.3B,C). The thermal plume can be defined as the zone where the thermal anomaly introduces significant phase distortion, so the plume boundary is defined as the point where the slope of the phase function changes abruptly (red markers in Fig.3B,C,E; black line in Fig.3A).

Shadowgraph estimated from DI: Without the lens into the beams pathway (Fig.1), the interference figure would be superposed on a shadowgraph figure, and the borders of the plume indicated by the shadowgraph would correspond to the maximum slope in the phase function (i.e. maximum of the first derivative of the phase function or the second derivative of the refractive index projection; black markers in Fig.3D). Shadowgraph has often been used to measure the size of the plume cap [4,5]. The white line in Fig.3A shows the contour of the "plume" as seen by shadowgraph: plume dimensions measured by shadowgraph are underestimated.

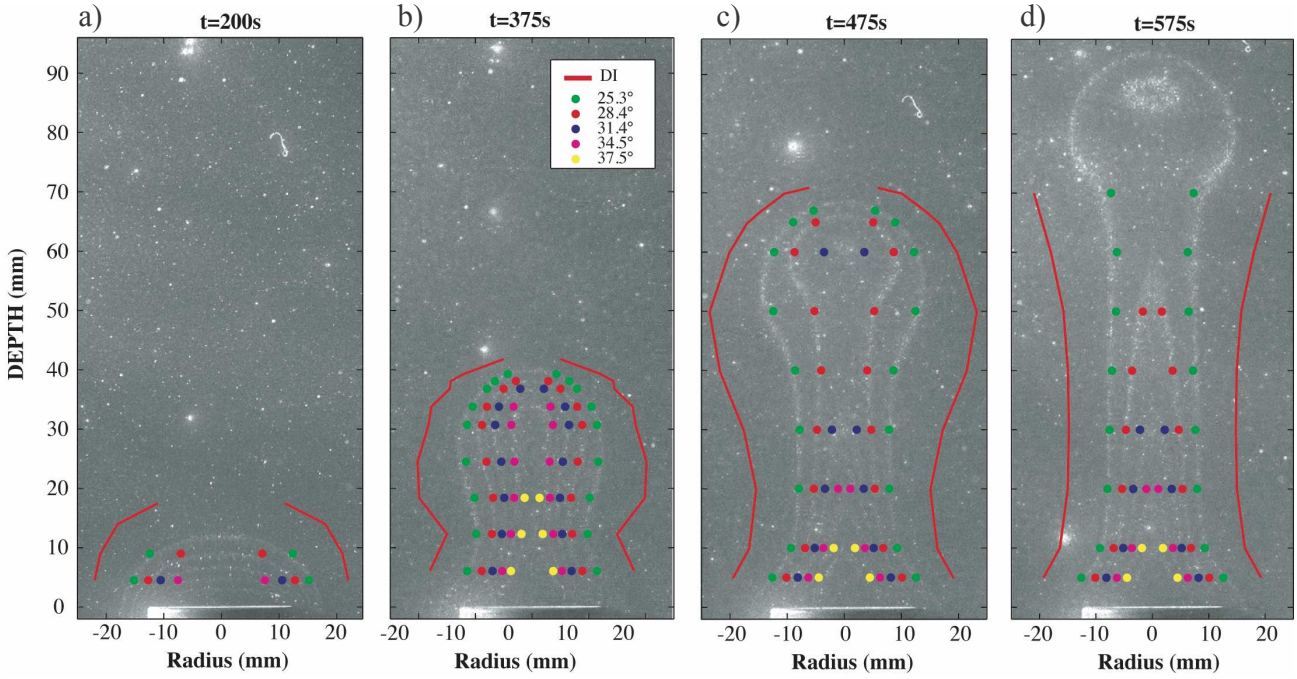

Fig.5: Comparison between the TCL images and the temperature field calculated from DI for glucose syrup at for different moments of the plume evolution. The points are obtained by intersecting the DI temperature field to the discrete values of the isotherms. Red line indicates the DI plume boundary.

TLCs: The development of the plume is shown by isotherms (Fig.5, 6). The quality of the TLC images for silicone oil is poorer than for glucose syrup (narrower, brighter stripes), as expected from the calibration (Fig.4, Table 2).
Comparison DI vs.TLCs: Figs. 5-6 show plume evolution TLC images superposed with the corresponding data for several heights measured by DI method. For sugar syrups, there is an excellent agreement at all times (Fig.5). For silicone oil, the agreement is good at early stages of plume development (Fig.6a,b) but at later stages, (Fig.6c) the isotherms appear to be shifted upwards (i.e. in the flow direction) compared to the temperature structure determined by DI. This seems to indicate that the response time of the oil TLCs is too slow compared to the transit time of the TLC capsule at a given temperature in the plume.

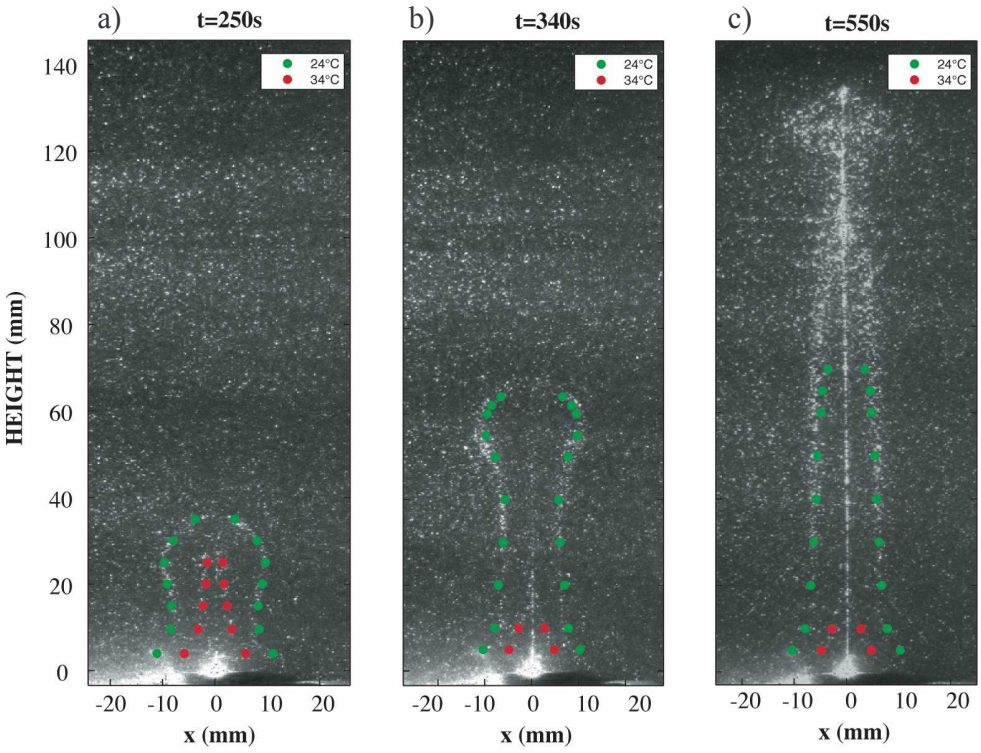

Fig.6: Comparison between the TCL images and the temperature field calculated from DI for silicone oil at three different moments of the plume evolution.

DI has the advantage to give the complete temperature field upon inversion of the interferograms. Its disadvantages are that a) the dimension of the investigated object depends on the expansion beam diameter which is limited by the optics (here only 80 mm diameter), b) since the test region is imaged, the position of the thermal anomaly has to be well determined in advance and c) it cannot be used quantitatively for geometries which are neither 2D nor axisymmetric. In our case, for axisymmetric and steadily rising plume, one can however overcome (a) by following the plume cap by elevating both the laser and cameras on the tables. The results for a thermal plume in glucose syrup are shown in Mov.3.
The TLC method has the advantages of a) direct visualization of some discrete isotherms, b) a simple setup with a visualization cross-section which can encompass the whole experimental tank (a simple

cylindrical lens can produce almost any dimensions for the laser sheet), c) laser scanning system allows imaging fully 3D thermal anomalies since no axisymmetric hypothesis is needed [13,14], d) a simple calibration procedure which can allow isotherms determination with a 0.1°C precision for aqueous solutions. However, TLCs response time can become a problem. And the biggest disadvantage of this TLC method remains that only a few isotherms are measured.

3.2 Plume dynamics

We can now focus on the development of a thermal plume issued from a finite size heater.

A plume development in three stages:
Once the heater is turned on, a thermal boundary layer (TBL) grows over it by heat conduction ("Stage I", Fig.5a). When the Stokes velocity of this hot pocket becomes greater than its growth by heat diffusion, a thermal starting plume is generated [5]. The hot plume has the classical "mushroom" (spherical head + tail) structure (Fig.5b-d) since, due to temperature-dependent viscosity, hot material has a lower viscosity than the ambient fluid. At first, plume dynamics is dominated by this plume head, which behaves as a thermal ("stage II"). The head cools through time by thermal diffusion; we can see that the hotter isotherms in the head are disappearing one after another. In the end the TLC images show a steady stem, "cigar" like, and plume dynamics is controlled by the stem ("stage III").

The height of the plume head has been evaluated by the two methods: the "zero thermal anomaly boundary" measured by DI, and the height of each TLC isotherm. Their temporal evolution is shown in Fig.7. The shape of each isotherm depends on the absolute value of the initial temperature of the fluid, while the shape of the differential interferometry image depends only on the relative temperature anomaly. So each isotherm follows the DI head evolution until the plume head has cooled enough. Then each isotherm, after a given time, will be located only in the plume stem (stage III). At a given height, the stem is becoming steady right after the passage of the head (Figs.5-7). On the other hand, the DI-determined head height will continue to rise as long as a thermal anomaly exists. It is therefore a more reliable method for plume size determination.

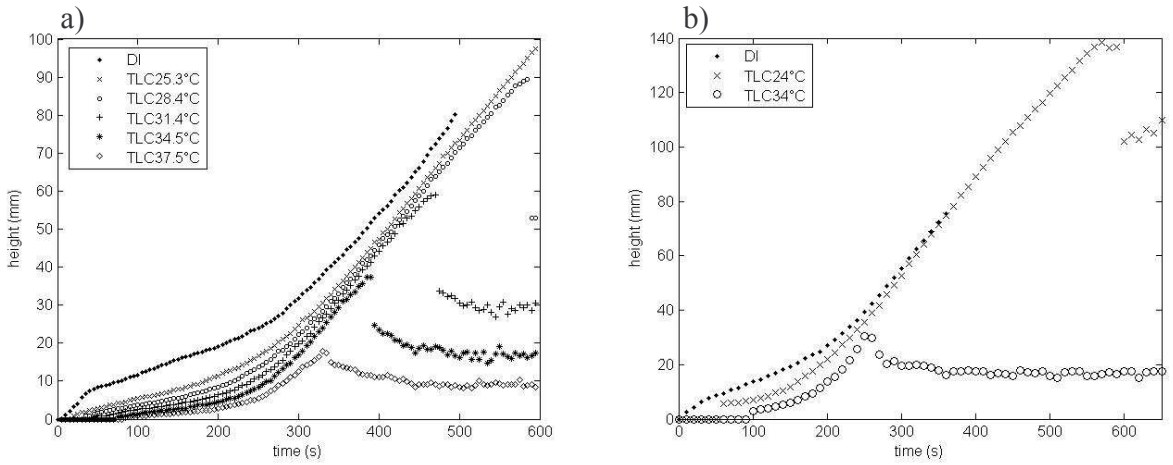

Fig.7: The height of the plume measured by DI and TLC. a) sugar syrup, b) silicone oil.

Scalings in the steady-state stem:

Figures 5-7 show that the plume stem thermal structure remains constant as soon as it is built: the stem quickly achieves a steady-state structure that is independent of the dynamics of the ascending head above. Since we have the complete temperature field, we can test the scalings which have been proposed for constant viscosity plume stem [15,16], and strongly temperature-dependent viscosity plume [17].

Batchelor [15] considered a model in which a plume rises from a point source of heat of power P in an infinite fluid with constant properties and high Prandtl number. Simple scaling arguments suggest that the temperature anomaly ΔT, and the stem radius R scale with the height z above the source as:

$$\Delta T \sim \frac{P}{\kappa \rho C_p z}, \qquad R \sim \left(\frac{\rho C_p \nu \kappa^2}{g \alpha P} \right)^{1/4} z^{1/2} \tag{3}$$

Thermal diffusion causes the temperature anomaly to decrease with height as z^{-1} and the stem radius to increase as $z^{1/2}$. Experiments in water (Pr~7) verify the scalings (3) if corrections are made for the finite size of the heat source and for downward heat losses from it: this is done by replacing in (3) z by $(z-z_0)$ where z_0 is the origin of a real point source equivalent to our finite size source [16]. Fig.8a presents the radial temperature structure of the stem for several heights. When the scalings according to Eq.(3) are applied, all the curves sufficiently far from the source collapse on top of each other (Fig.8b, for height greater than 20 mm) if z_0 = -4mm.

For the steady flow above a point source of heat in a fluid whose viscosity depends exponentially on temperature, Olson et al. [17] derived an approximate solution of the boundary-layer equations which gives:

$$\Delta T = \Delta T_0 \exp\left(\frac{-4\pi k \Delta T_r z}{P} \right), \quad R = \left(\frac{2}{\rho \Delta T_r} \right)^{1/2} \left(\frac{P \rho \nu_0(z)}{\pi \alpha g C_P} \right)^{1/4} \tag{4}$$

where $\nu_0(z)$ is the viscosity on the plume centerline, ΔT_0 is the temperature anomaly at the base of the plume, k is the thermal conductivity, and ΔT_r is the temperature required to change the viscosity by a factor e. The temperature anomaly decreases exponentially with height. The differences relative to the constant-viscosity case are due to the fact that temperature-dependent viscosity concentrates the upwelling in the hottest central part of the plume stem, so that the radius δ_T of the thermal anomaly is wider than the radius δ_w of the upwelling region (the "conduit" proper) even for Pr >>1. This situation is opposite to the constant viscosity case at high Pr. Fig.8c presents the radial temperature structure of the stem for several heights. When the scalings according to Eq.(4) are applied (Fig.8d), the curves sufficiently far from the source (for height greater than 10 mm), and for temperature anomaly greater than ΔT_r (for height lower than 60 mm), collapse on top of each other. In the case of this sugar syrup, Olson's scaling predicts well the data if the local viscosity ratio (between the stem axis and the far-field fluid) is greater than 2.2.

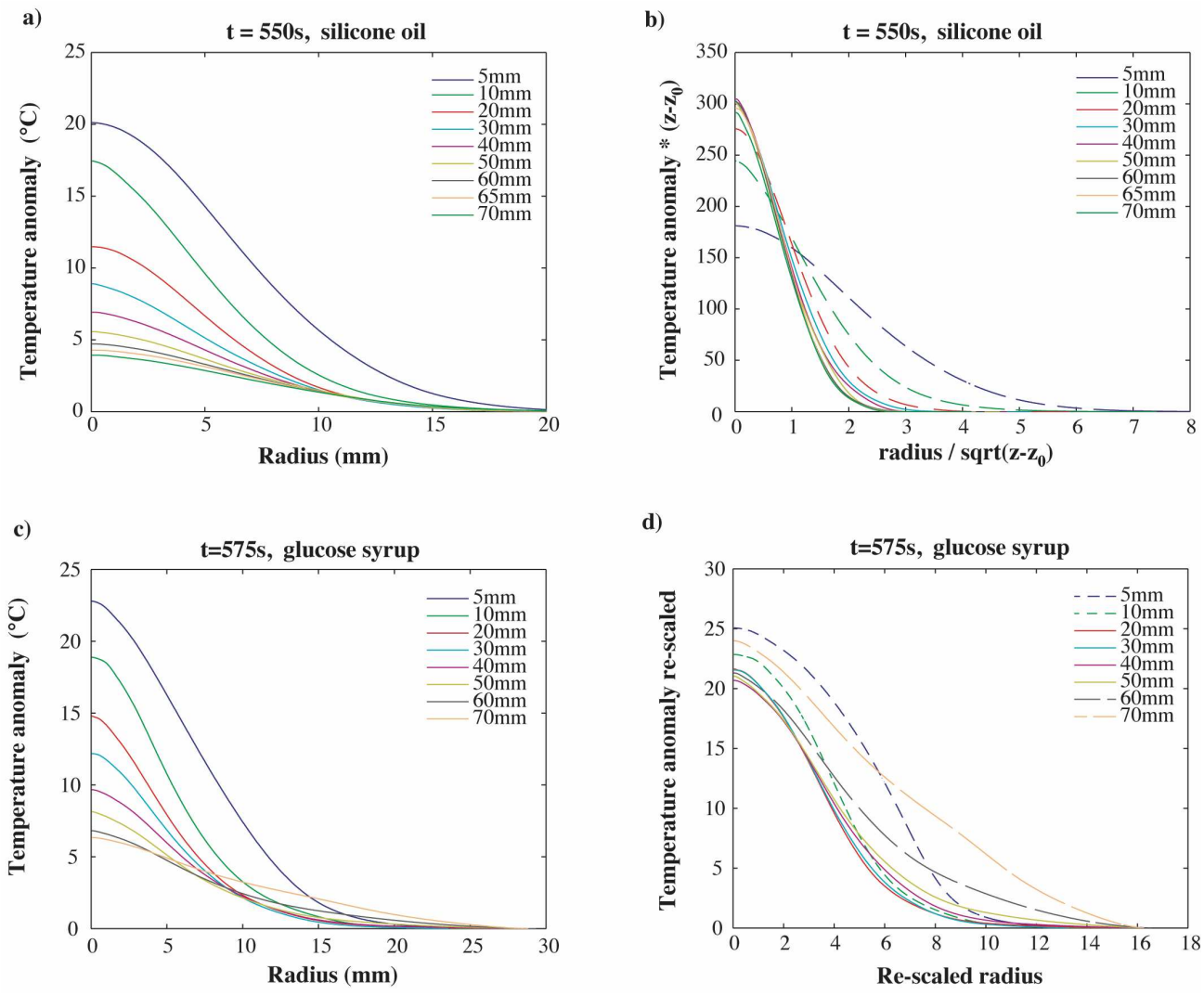

Fig.8: The temperature field measured by DI: a) Plume temperature anomaly in silicone oil at t=550°C, b) Same as a) but scaled according to Eq.(3), c) Plume temperature anomaly in glucose syrup at t=575s, d) Same as c) but scaled according to Eq.(4).

References

1. Davaille A and Limare A. Laboratory Studies in Mantle Convection in Treatise of Geophysics, volume editor D. Bercovici, editor G. Schubert, Elsevier, 89-165, 2007.
2. Griffiths RW and Campbell IH. Stirring and Structure in mantle starting plumes. *Earth Planet. Sci. Lett.* 99, 66-78, 1990
3. Coulliette DL and Loper DE. Experimental, numerical and analytical models of mantle starting plumes. *Phys. Earth Planet. Inter.* 92, 143-167, 1992.

4. Moses E, Zocchi G, and Libchaber A. An experimental study of laminar plumes. *J. Fluid Mech.* 251, 581-601, 1993.
5. Kaminski E and Jaupart C. Laminar starting plumes in high-Prandtle-number fluids. *J. Fluid Mech.* 478, 287-298, 2003.
6. Kumagai I, Davaille A and Kurita K. On the fate of thermally buoyant mantle plumes at density interfaces. *Earth Planet. Sci. Lett.* 254, 180-193, 2007.
7. Kelley JG and Hargreaves RA. A rugged inexpensive shearing interferometer. *Applied Optics*, 9, 948-952, 1970.
8. Vest CM. Interferometry of strongly refracting axisymmetric phase objects. *Applied Optics*, 14, 1601-1606, 1975.
9. Rhee H, Koseff J and Street R. Flow visualization of a recirculating flow by rheoscopic and liquid crystal techniques. *Exp. Fluids*, 2, 57–64, 1984.
10. Dabiri D and Gharib M. Digital particle image thermometry: the method and implementation, *Exp. Fluids*, 11, 77–86, 1991.
11. Willert C and Gharib M. Digital Particle Image Thermometry, *Exp. Fluids*, 10, 181–193, 1991.
12. Fujisawa, N., and R. Adrian, Three-dimensional temperature measurement in turbulent thermal convection by extended range scanning liquid crystal thermometry, J.Visualization, 1, 355–364, 1999
13. Le Bars M and Davaille A. Stability of thermal convection in two superimposed miscible viscous fluids. *J Fluid Mech* 471:339–363, 2002.
14. Davaille A and Vatteville J. On the transient nature of mantle plumes. *Geophys Res Lett,* 32, doi:10.1029/2005GL023029, 2005.
15. Batchelor GK. Heat convection and buoyancy effects in fluids. *Q.J.R.Met.Soc.* 80, 339—358, 1954.
16. Shlien DJ and Boxman RL. Temperature field measurement of an axisymmetric laminar plume. *Phys. Fluids* 22, 631-634, 1979.
17. Olson P, Schubert G and Anderson C. Structure of axisymmetric mantle plumes. *J Geophys Res* 98, 6829–6844, 1993.

Movies

Movie 1: Thermal plume evolution in glucose syrup by DI and TLC methods.
Movie 2: Thermal plume evolution in silicone oil by DI and TLC methods.
Movie 3: DI monitoring of a thermal plume.

Copyright Statement